

# Image denoising using the Gaussian curvature of the image surface

Carlos Brito-Loeza\*, Ke Chen<sup>†</sup> and Victor Uc-Cetina\*

## Abstract

A number of high order variational models for image denoising have been proposed within the last few years. The main motivation behind these models is to fix problems such as the staircase effect and the loss of image contrast that the classical Rudin-Osher-Fatemi model [*Phys. D*, 60 (1992), pp. 259–268] and others also based on the gradient of the image do have. In this work, we propose a new variational model for image denoising based on the Gaussian curvature (GC) of the image surface of a given image. We analytically study the proposed model to show why it preserves image contrast, recovers sharp edges, does not transform piecewise smooth functions into piecewise constant functions and is also able to preserve corners. In addition, we also provide two fast solvers for its numerical realization. Numerical experiments are shown to illustrate the good performance of the algorithms and test results.

AMS subject class: 68U10, 65F22, 65K10.

Keywords: Denoising, variational models, regularization, augmented Lagrangian method.

## 1 Introduction

Image denoising is the technique used to approximate a true image from an observed noisy image. There exist many different ways to achieve this goal. For instance, spatial linear filtering [19], linear and nonlinear anisotropic filtering using a partial differential equation (PDE) [25, 35], Wavelet-based methods [36, 13, 14], Markov-Random-Field-based methods [34] and variational methods [28, 1] just to mention a few have been proposed in the past.

Among variational methods, maybe the most popular and deeply analyzed model is the Total Variation (TV) image denoising model also known as the ROF model [26]. Although, on one hand, this model is extremely good in

---

\*C. Brito-Loeza and V. Uc-Cetina are with Facultad de Matemáticas, Universidad Autónoma de Yucatán, México. (Emails: carlos.brito@uady.mx and ucetina@uady.mx)

<sup>†</sup>K. Chen is with Centre for Mathematical Imaging Techniques and Department of Mathematical Sciences, University of Liverpool, Liverpool L69 7ZL, United Kingdom (Email: K.Chen@liv.ac.uk; web: www.liv.ac.uk/cmit).

removing noise and preserving edges and image contours, on the other hand, it makes smooth regions of the images to look blocky creating a visually unpleasant effect and has also the tendency to reduce the image contrast of low scale objects [30]. We note that a Bregman based approach [18] can improve the restoration in a large extent but not in theory. In this paper, we propose a new high order model based on the Gaussian curvature of the image surface. We will show analytically in a future section that our model does not suffer from the aforementioned problems and still is capable of removing noise fairly from the image while keeping edges and contours sharp.

Our model finds its foundations in the recent works: [22] where some curvature approximation is used for image denoising, [6] where mean curvature (MC) is used for surface fairing, the work in [41] where MC of the image surface is proposed for 2-D denoising and [15] where the analogue of the total variation denoising model in the context of geometry processing is introduced. On one hand [6, 22, 41], are successful examples of a high order models sharing many of the good properties already mentioned for our model. In fact, we will use through out this manuscript some of the techniques developed in [41] to prove some of our arguments. On the other hand, up to our knowledge, [15] is the very first work to introduce the Gaussian curvature of the surface as a tool to develop a variational model for geometric processing.

A very frequent occurring type of noise in nature is additive and has Gaussian probability distribution with zero-mean and given variance  $\sigma$ . Therefore a noisy image can be mathematically modeled with the equation

$$f(x, y) = u(x, y) + \eta(x, y) \quad (1)$$

where  $f = f(x, y)$  is the known noisy image,  $u = u(x, y)$  is the unknown true image and  $\eta = \eta(x, y)$  is the unknown additive noise all of them defined on a domain  $\Omega \subseteq \mathbb{R}^2$ . From the variational point of view, the task of removing noise can be accomplished by solving a minimization problem such as

$$\min_u \left\{ \int_{\Omega} (f - u)^2 \, dx dy + \alpha R(u) \right\} \quad (2)$$

where  $\alpha > 0$  is a tuning parameter which can be optimized if the underlying noise variance is estimated [40] and  $R(u)$  a given regularizer. Maybe the most popular selection so far for the regularizer  $R(u)$  is the total variation of  $u$  defined as  $\int_{\Omega} |\nabla u| \, dx dy$ . This regularizer was proposed for the denoising ROF model in [26]. The ROF model yields very good results when the image is piecewise constant by being capable of removing image noise while preserving edges of objects. However, it also has some well known drawbacks such as the loss of image contrast and the staircase effect, the latter very unfortunate when the true image is smooth or piecewise smooth causing the restored image to have some artifacts and to look blocky. Although some effort has been made [23, 27, 12] to numerically reduce the staircase effect, some researchers just recently started turning to higher order models looking for better solutions. In this direction are for instance the works presented in [39, 22, 21] which tested different ways of

combining second order derivatives in the regularizer, MC-based models [6, 41] which use the  $L_1$  norm of the MC as regularizer and the Total Generalized Variation (TGV) model [5] which is based on obtaining the optimal balancing between the first and second derivative of the image. Consequently, this model prefers piecewise smooth images over staircase images in terms of penalization.

In particular, there are two models, [41] and [7], both based on a well known geometric entity: mean curvature, which are closest to ours. These two models differ on that [41] use as regularizer the MC of the surface implicitly generated by the image while [7] use the MC of the level lines of the image. The popularity of mean curvature has grown within the last years because in addition to removing noise, is also able to keeping edges and contours of objects sharp and to preserving corners, smooth regions and image gray-scale intensity contrasts as well. Mean curvature based regularizers have been proposed for different imaging applications. For instance, in [41] for image denoising, [10] for image registration, [8, 24] for image inpainting, and [42] for segmentation.

## 1.1 Review

We will review in more detail the two models that we have identified as closest to ours: the image denoising model using the mean curvature of the image surface [41] and the image denoising model using the curvature of the level-lines of the image [7].

The model introduced by Zhu and Chan in [41] is based on the curvature of the surface  $S$  induced by some image  $u(x, y)$  through the mapping  $(x, y, u(x, y))$ . The authors in [41] defined their 2-D variational image denoising model as the following minimization problem:

$$\min_u \left\{ \int_{\Omega} (f - u)^2 \, dx dy + \alpha \int_{\Omega} |\kappa_M| \, dx dy \right\}. \quad (3)$$

where

$$\kappa_M = \nabla \cdot \left( \frac{\nabla u}{\sqrt{|\nabla u|^2 + 1}} \right). \quad (4)$$

A related but different model was proposed in [21] where curvature is approximated and not solved directly. The model (3) was studied in [7] by using the curvature of the image level lines

$$\kappa_M = \nabla \cdot \left( \frac{\nabla u}{\sqrt{|\nabla u|^2 + \epsilon}} \right) \quad (5)$$

where the regularizing parameter  $\epsilon$  has been added to avoid division by zero.

It is clear that both models, [7] and [41], are the same when  $\epsilon \rightarrow 1$ . This apparently slight change has dramatic effects to the model's solution. On one hand, small  $\epsilon$  let us to recover sharp edges easily but on other hand the numerical solution gets much harder to obtain by means of the classical methods. In

[7] a fast nonlinear multigrid method was developed for both models but its performance showed to be much better for [41] than for [7]. A simple explanation maybe found looking at the ellipticity of  $\kappa_M$ . When  $\epsilon = 1$  the ellipticity of  $\kappa_M$  is much larger than that obtained when  $\epsilon \rightarrow 0$ . The ellipticity of the diffusion PDE one needs to solve either for [41] or [7] depends strongly on  $\kappa_M$  therefore multigrid methods will perform much better in the former case.

The above observation prompted the motivation of looking for a new model in between the former two but at the same time sharing their nice properties: large ellipticity and sharp reconstructions.

The use of geometric entities to create new variational models maybe an advantage since all tools from the field of differential geometry are available to us helping to get a better insight of these models. There are also good solvers for (3), for instance: the augmented Lagrangian method from [43], the nonlinear multigrid method proposed in [7, 10], the homotopy method from [16] and the iterative method from [29].

Mean curvature has already been used in a different way to denoise an image. Recently, Bertalmío and Levine [4] showed that when an image is corrupted by additive noise, the curvature of the level sets of the image is less affected by it. Based on this observation, they designed a method to obtain better results by applying it to the curvature image and then reconstructing from it a clean image, rather than denoising the original image directly. Although they used mean curvature, we believe that Gaussian curvature would be a good candidate as well. In that sense, the model we propose here could be adapted to Bertalmío and Levine's model. Also related is the model from [31] where the authors proposed a compound denoising model fo first and second order derivatives.

A related work to image denoising using the curvature of the image surface is the surface fairing model presented by Elsey and Esedoglu [15]. There the authors proposed the analogue of the total variation denoising model in the context of geometry processing by defining a new regularizer based on the Gaussian curvature of a closed surface and using it to remove noise in 3D objects. Their model preserves sharp edges and corners such as the MC model does in 2D denoising. Hence, a natural question arises from here: Is the Gaussian curvature based regularizer suitable for image denoising? The objective of this paper is to provide an answer to this question.

The outline of this paper is as follows. In §2 we introduce the new Gaussian curvature based regularizer. In §3 we carry out the analysis of the proposed model. In §4 two different iterative methods: the two-step (TS) method and the augmented Lagrangian (ALM) method are proposed for the numerical solution of the GC model. In §5, we present experimental results to highlight the virtues of the model and numerical evidence to show the very good performance of both numerical algorithms. Finally in §6 we present our conclusions.

## 2 The new Gaussian curvature regularizer for image denoising

As we explained in the previous section, and motivated by the good results of the 3D fairing model of Elsey and Esedoglu, we explore here a GC based model for 2D image denoising.

The GC of a 3D surface  $S$  represented implicitly by the zero level set function  $\phi$  is given by

$$\kappa_G = \frac{\nabla\phi H^*(\phi)\nabla\phi^T}{|\nabla\phi|^4} \quad (6)$$

where  $\nabla\phi = (\phi_x, \phi_y, \phi_z)$  is the gradient vector,  $|\nabla\phi| = \sqrt{\phi_x^2 + \phi_y^2 + \phi_z^2}$  the gradient norm,

$$H(\phi) = \begin{pmatrix} \phi_{xx} & \phi_{xy} & \phi_{xz} \\ \phi_{yx} & \phi_{yy} & \phi_{yz} \\ \phi_{zx} & \phi_{zy} & \phi_{zz} \end{pmatrix} \quad \text{and}$$

$$H^*(\phi) = \begin{pmatrix} \phi_{yy}\phi_{zz} - \phi_{yz}\phi_{zy} & \phi_{yz}\phi_{zx} - \phi_{yx}\phi_{zz} & \phi_{yx}\phi_{zy} - \phi_{yy}\phi_{zx} \\ \phi_{xz}\phi_{zy} - \phi_{xy}\phi_{zz} & \phi_{xx}\phi_{zz} - \phi_{xz}\phi_{zx} & \phi_{xy}\phi_{zx} - \phi_{xx}\phi_{zy} \\ \phi_{xy}\phi_{yz} - \phi_{xz}\phi_{yy} & \phi_{yx}\phi_{xz} - \phi_{xx}\phi_{yz} & \phi_{xx}\phi_{yy} - \phi_{xy}\phi_{yx} \end{pmatrix}^T$$

are the Hessian matrix  $H(\phi)$  and its adjoint  $H^*(\phi)$ . The derivation of this formula can be found in [17].

Consider an image function  $u(x, y)$  and think of  $S$  as the graph of  $u$ . Then we can use the relation  $\phi = u(x, y) - z$  to get a formula for  $\kappa_G$ . With this new set of coordinates, the gradient is given by  $\nabla\phi = (u_x, u_y, -1)^T$  and the Hessian and its adjoint can be expressed as follows

$$H(\phi) = \begin{pmatrix} u_{xx} & u_{xy} & 0 \\ u_{yx} & u_{yy} & 0 \\ 0 & 0 & 0 \end{pmatrix},$$

$$H^*(\phi) = \begin{pmatrix} 0 & 0 & 0 \\ 0 & 0 & 0 \\ 0 & 0 & u_{xx}u_{yy} - u_{xy}u_{yx} \end{pmatrix}.$$

Therefore the Gaussian curvature of the image surface reads

$$\kappa_G = \frac{u_{xx}u_{yy} - u_{xy}u_{yx}}{(u_x^2 + u_y^2 + 1)^2}. \quad (7)$$

Now we are ready to formulate our new model using the functional

$$R(u) = \int_{\Omega} \left| \frac{u_{xx}u_{yy} - u_{xy}u_{yx}}{(u_x^2 + u_y^2 + 1)^2} \right| dx dy \quad (8)$$

as a regularizer. Note that the numerator in the definition of  $\kappa_G$  is equal to the determinant of the Hessian of  $u$ . Therefore the new image denoising model based on the GC of the image surface may be written as

$$\min_u E(u) = \left\{ \int_{\Omega} (f - u)^2 dx dy + \alpha \int_{\Omega} \left| \frac{\det(H(u))}{(|\nabla u|^2 + 1)^2} \right| dx dy \right\}. \quad (9)$$

To find the solution of the GC model, ones has to solve the Euler-Lagrange equation

$$\alpha \nabla \cdot \left( \frac{4|u_{xx}u_{yy} - u_{xy}u_{yx}|}{\mathcal{N}^3} \nabla u \right) + \nabla \cdot \mathbf{B}_1 + \nabla \cdot \mathbf{B}_2 + u - f = 0 \quad (10)$$

with boundary conditions

$$(-u_{xy}, u_{xx}) \cdot \boldsymbol{\nu} = 0, (u_{yy}, -u_{yx}) \cdot \boldsymbol{\nu} = 0, -\mathbf{B}_1 \cdot \boldsymbol{\nu} = 0, \text{ and } -\mathbf{B}_2 \cdot \boldsymbol{\nu} = 0$$

where definitions for  $\mathbf{B}_1$  and  $\mathbf{B}_2$  along with derivation of this PDE can be found in Appendix A.

In the following section we will analyze some properties of the GC model. However at this moment we have no mathematical proof of the existence and uniqueness of its solution remaining an open problem.

### 3 Analysis of the model

It is important to show that our proposed model (9), provided some conditions are satisfied, is able to preserve image contrast, edges and corners such as the MC model does. To achieve this, we will extend the results from [41] for the MC model to the new GC model and highlight steps unique to it.

#### 3.1 Contrast preservation

In order to show that the GC regularizer preserves image contrast, we need to prove that it does not depend on the brightness of image objects here represented by  $h$ . To this end, we adopt the analysis method of [41].

- Consider a sharp image  $f = h\chi_{B(0,R)}$  defined on a rectangle  $\Omega = (-2R, 2R) \times (-2R, 2R)$ , where  $\chi$  is the characteristic function,  $B(0, R)$  is an open disk in  $\mathbb{R}^2$  centered at the origin with radius  $R$  and  $h > 0$ .
- Consider the set  $S$  of functions defined as

$$S = \left\{ g \in C^2[0, 2R] : g''(x) \leq 0 \text{ if } x \in (0, R), g''(x) \geq 0 \text{ if } x \in (R, 2R); \right. \\ \left. \text{there exist } R_1, R_2, 0 < R_1 < R < R_2 < 2R, \text{ such that} \right. \\ \left. g(x) = h \text{ if } x \in [0, R_1] \text{ and } g(x) = 0 \text{ if } x \in [R_2, 2R]; g'(R) < -2h/R \right\}.$$

where  $g \in S$  is a one variable function which generates an image surface by rotating about the vertical axis. The resulting rotating function defines

an image surface  $(x, y, u(x, y))$  in terms of  $g$  through  $u(x, y) = g(r)$  with  $r = \sqrt{x^2 + y^2}$ . From  $S$ , we can choose a convenient sequence of radial symmetric smooth functions  $g$  whose revolution surfaces approach the graph of  $f$ .

One way to construct such a sequence of functions  $g$  is by using the sigmoidal function  $g(x) = h/(1 + \exp(-a(x - c)))$  where  $h, c$  are constants and letting  $a \rightarrow \infty$ . We illustrate this in Figure 1. Clearly as  $a$  grows, the revolution surface approximates the graph of  $f$ .

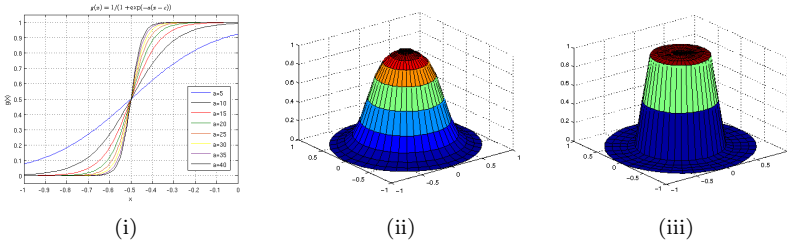


Figure 1: (i) Family of  $g$  functions obtained with  $g(x) = h/(1 + \exp(-a(x - c)))$  where  $h = 1, c = -0.5$  and  $a$  varying from 5 to 40. (ii) - (iii) Revolution surfaces obtained by rotating  $g$  over the  $z$  axis with  $a = 15$  and  $a = 40$  respectively.

- The GC regularizer for the chosen sequence will be computed and the limit taken to show that  $\int \kappa_G(f)$  does not depend on  $h$ .

In the Appendix B, it is shown that the GC can be expressed in terms of  $g$  as follows:

$$\kappa_G = \frac{u_{xx}u_{yy} - u_{xy}u_{yx}}{(1 + u_x^2 + u_y^2)^2} = \frac{g'g''}{r(1 + (g')^2)^2}. \quad (11)$$

Hence,

$$\begin{aligned} \int |\kappa_G| dx dy &= \int_0^{2\pi} d\theta \int_0^{2R} r |\kappa_G| dr \\ &= 2\pi \int_0^{2R} r \left| \frac{g'g''}{r(1 + (g')^2)^2} \right| dr \\ &= 2\pi \int_0^{2R} \left| \frac{g'g''}{(1 + (g')^2)^2} \right| dr. \\ &= \pi \int_0^{2R} \left| - \left( \frac{1}{1 + (g')^2} \right)' \right| dr. \end{aligned} \quad (12)$$

To compute (12) we proceed by splitting the integral over the two intervals  $[0, R]$  and  $[R, 2R]$ .

First, when  $r \in [0, R]$ ,  $g'(0) = 0$ ,  $g' \leq 0$ ,  $g'' \leq 0$  therefore  $\kappa_G \geq 0$  and

$$\begin{aligned} \int |\kappa_G| dx dy &= -\pi \int_0^R \left( \frac{1}{1+(g')^2} \right)' dr \\ &= -\pi \left( \frac{1}{1+(g'(R))^2} - \frac{1}{1+(g'(0))^2} \right) \\ &= \frac{-\pi}{1+(g'(R))^2} + \pi. \end{aligned} \quad (13)$$

Second, when  $r \in [R, 2R]$ ,  $g'(2R) = 0$ ,  $g' \leq 0$ ,  $g'' \geq 0$  therefore  $\kappa_G \leq 0$  and

$$\begin{aligned} \int |\kappa_G| dx dy &= \pi \int_R^{2R} \left( \frac{1}{1+(g')^2} \right)' dr \\ &= \pi \left( \frac{1}{1+(g'(2R))^2} - \frac{1}{1+(g'(R))^2} \right) \\ &= \frac{-\pi}{1+(g'(R))^2} + \pi. \end{aligned} \quad (14)$$

Hence for  $r \in [0, 2R]$ ,

$$\int |\kappa_G| dx dy = \frac{-2\pi}{1+(g'(R))^2} + 2\pi. \quad (15)$$

However as the revolution surface generated with  $g$  approaches the graph of  $f$ ,  $g'(R) \rightarrow \infty$  yielding

$$\int |\kappa_G| dx dy = 2\pi. \quad (16)$$

The last equation, means that the regularizer based on the GC of the image surface does not depend on  $h$ , therefore it is invariant to changes in the gray level intensities. Our model shares this property with the mean curvature regularizer.

### 3.2 Edge preservation

We now show that the GC model preserves edges. To show edge preservation we need to demonstrate that  $E(f) < E(g)$  for  $g \in S$ . Note that  $E(g)$  is defined as

$$E(g) = \alpha \int |\kappa_G| dx dy + \int (f - g)^2 dx dy. \quad (17)$$

The result from [41] gives

$$\int (f - g)^2 dx dy \geq -\frac{\pi h^3 R}{12g'(R)}.$$

Hence we only need to focus on the regularization term. From (15) we already know that

$$\int |\kappa_G| dx dy = \frac{-2\pi}{1 + (g'(R))^2} + 2\pi.$$

Therefore the following inequality is true

$$\begin{aligned} E(g) &> \alpha \left( \frac{-2\pi}{1 + (g'(R))^2} + 2\pi \right) - \frac{\pi h^3 R}{12g'(R)} \\ &= \alpha \left( \frac{-2\pi}{1 + (-g'(R))^2} + 2\pi \right) + \frac{\pi h^3 R}{12(-g'(R))}. \end{aligned} \quad (18)$$

Now define  $s = -g'(R)$  and consider

$$\begin{aligned} \zeta(s) &= \alpha \left( \frac{-2\pi}{1 + s^2} + 2\pi \right) + \frac{\pi h^3 R}{12s} \\ &= \alpha 2\pi \left( \frac{s^2}{1 + s^2} \right) + \frac{\pi h^3 R}{12s}. \end{aligned} \quad (19)$$

Note that by definition the domain of  $\zeta$  is the interval  $[\frac{2h}{R}, +\infty)$ . By defining  $C_1 = 2\pi$  and  $C_2 = \frac{\pi h^3 R}{12}$  we obtain

$$\zeta(s) = \frac{\alpha C_1 s^2}{1 + s^2} + \frac{C_2}{s} \quad (20)$$

and

$$\lim_{s \rightarrow \infty} \zeta(s) = \lim_{s \rightarrow \infty} \frac{\alpha C_1 s^2}{1 + s^2} + \frac{C_2}{s} = \alpha C_1. \quad (21)$$

Further,

$$\begin{aligned} \zeta'(s) &= \frac{2\alpha C_1 s}{(1 + s^2)^2} - \frac{C_2}{s^2} \\ &< \frac{2\alpha C_1}{s^3} - \frac{C_2}{s^2} \\ &= \frac{2C_1}{s^3} \left( \alpha - \frac{C_2}{2C_1} s \right). \end{aligned} \quad (22)$$

Thus selecting  $\alpha < \frac{C_2}{2C_1} \frac{2h}{R}$  we find that  $\zeta'(s) < 0$  for any  $s \in [\frac{2h}{R}, +\infty)$ . In other words, provided  $\alpha$  is less than

$$\alpha_{max} < \frac{C_2}{2C_1} \frac{2h}{R} = \frac{h^4}{24}, \quad (23)$$

$\zeta(s)$  is decreasing with limit  $\alpha C_1$  implying  $E(g) > \alpha C_1$ .

From (16) and (17)

$$E(f) = 2\pi\alpha = \alpha C_1 < E(g) \quad (24)$$

for any  $g \in \mathcal{S}$ . From here, using the same arguments to those presented in [41], for any small  $\epsilon > 0$ , we can find a smooth function  $g \in \mathcal{S}$  such that  $E(g) - \epsilon < E(f) < E(g)$  hence  $E(f) = \inf_{u \in \mathcal{S}} E(u)$ .

Since  $f$  is a sharp object, this proves that the GC model preserves sharp edges. In addition, this also shows that for rightly selected  $\alpha$ , the image contrast of  $f$  is preserved.

### 3.3 Corner preservation

To show corner preservation, we follow a similar procedure to the one used before for contrast preservation. This time, however, a sharp image  $f = h\chi_Z$  is defined on a rectangle  $\Omega = (-R, R) \times (-R, R)$  with  $Z = (0, R) \times (0, R)$ . The image  $f$  is therefore a square with brightness  $h$  or a rectangular parallelepiped when viewed as a 3-D surface.

To generate the new image surface  $(x, y, \zeta(x, y))$  we have to redefine both: the one variable function  $g$  and the set  $S$ . To this end, let

$$S = \left\{ g \in C^2(\mathbb{R}) : g(x) = 0 \text{ if } x < -1, g(x) = 1 \text{ if } x > 1; \right. \\ \left. g'' \geq 0 \text{ in } (-1, 0), g'' \leq 0 \text{ in } (0, 1); \text{ and } 1 \leq g'(0) \leq 2 \right\} \quad (25)$$

and define  $\zeta(x, y)$  in terms of  $g$  through

$$\zeta(x, y) = \begin{cases} hg\left(\frac{2y}{\epsilon}\right) & (x, y) \in [\epsilon, R) \times (-R, R) \\ hg\left(\frac{2x}{\epsilon}\right) & (x, y) \in (-R, \epsilon) \times [\epsilon, R) \\ hg\left(2 - \frac{2x}{\epsilon}\right) & (x, y) \in (-R, \epsilon) \times (-R, \epsilon) \end{cases} \quad (26)$$

with  $r = \sqrt{(x - \epsilon)^2 + (y - \epsilon)^2}$ .

From  $S$ , and choosing small enough  $\epsilon$ , we can construct a convenient sequence of smooth functions  $g$  to approximate the graph of  $f$ . The surface  $z = \zeta(x, y)$  constructed this way is sufficiently sharp around the edges  $\{x = 0, y \in [\epsilon, R)\}$  and  $\{y = 0, x \in [\epsilon, R)\}$  and the corner  $(0, 0)$ .

It is easy to see that  $g' \geq 0$  for  $\Omega_1 = [\epsilon, R) \times (-R, R)$ ,  $g'' \geq 0$  for  $[\epsilon, R) \times (-R, 0)$  and  $g'' \leq 0$  for  $[\epsilon, R) \times (0, R)$ . Therefore,

$$\int_{\Omega_1} |\kappa_G| dx dy = \int_{\epsilon}^R \left[ \int_{-R}^0 \kappa_G dy - \int_0^R \kappa_G dy \right] dx \\ = \frac{2(R - \epsilon)}{1 + \left[\frac{2h}{\epsilon} \rho'(0)\right]^2} \quad (27)$$

In similar fashion,  $g' \geq 0$  for  $\Omega_2 = (-R, \epsilon) \times [\epsilon, R)$ ,  $g'' \geq 0$  for  $(-R, 0) \times [\epsilon, R)$  and  $g'' \leq 0$  for  $(0, R) \times [\epsilon, R)$  and

$$\int_{\Omega_2} |\kappa_G| dx dy = \frac{2(R - \epsilon)}{1 + \left[\frac{2h}{\epsilon} \rho'(0)\right]^2} \quad (28)$$

By noticing that in the limit when  $\epsilon \rightarrow 0$ ,  $\rho'(0) \rightarrow \infty$  we find that  $\int |\kappa_G| dx dy = 0$  in both  $\Omega_1$  and  $\Omega_2$ . In the last sub-domain  $\Omega_3 = (-R, \epsilon) \times (-R, \epsilon)$  approximating the corner, at each point  $(x, y) \in \Omega_3$  at least one of the principal curvatures of the surface lies either on a flat region or an edge. Therefore without any calculation we can infer that  $\int_{\Omega_3} |\kappa_G| dx dy = 0$  again. This is, Gaussian curvature regularization not only is  $h$ -independent but has null value in this example as well.

Hence  $E(f) = \inf_{u \in \mathcal{Q}} E(u)$  and being  $f$  an object with sharp edges and a corner, this confirms that Gaussian curvature regularization preserves edges and corners. Although the analysis was done for a simple rectangular object aligned to the grid the previous result give an insight of the behavior of the GC regularizer when dealing with objects with corners.

## 4 Numerical solution

We now consider the numerical solution of model (9) i.e.

$$\min_u \left\{ \int_{\Omega} (f - u)^2 dx dy + \alpha \int_{\Omega} \left| \frac{\det(H(u))}{(|\nabla u|^2 + 1)^2} \right| dx dy \right\}$$

which has the Euler-Lagrange equation (10) i.e.

$$\alpha \nabla \cdot \left( \frac{4|u_{xy}u_{yx} - u_{xx}u_{yy}|}{\mathcal{N}^3} \nabla u \right) + \nabla \cdot \mathbf{B}_1 + \nabla \cdot \mathbf{B}_2 + u - f = 0$$

with boundary conditions

$$(-u_{xy}, u_{xx}) \cdot \boldsymbol{\nu} = 0, (u_{yy}, -u_{yx}) \cdot \boldsymbol{\nu} = 0, -\mathbf{B}_1 \cdot \boldsymbol{\nu} = 0, \text{ and } -\mathbf{B}_2 \cdot \boldsymbol{\nu} = 0$$

It can be appreciated that the above equation is a fourth order nonlinear PDE with diffusion coefficients yielding anisotropic diffusion. In our initial tests, using the simple gradient descent method as numerical solver, this equation showed to be very stiff. One way to solve it efficiently is to develop a multigrid method as in [7]. Here we consider alternative unilevel methods.

In what follows we will present two different and fast ways to obtain the numerical solution of the Gaussian curvature model. First we will show how to implement a proven method based on smoothing the noisy vector field generated from the noisy image and recovering the denoised gray level values by nonlinear interpolation. This two-step method has already proven successful in different scenarios [6, 2, 22, 33, 32]. Then we will move to introduce the augmented Lagrangian method for the GC model.

### 4.1 A two-step method based on vector field smoothing and gray level interpolation

Our first selection, is a method where a vector field is constructed from the noisy image, this vector field is smoothed and gray levels recovered by interpolation. These steps are repeated a number of times until a satisfactory result is obtained. At each step, a second order nonlinear PDE has to be solved.

In the case of the GC model, the two-step (TS) method is a cyclic process where the first step is to re-write the regularization part of (9) as a function of the unit vector  $\mathbf{N} = \nabla u / |\nabla u|$  and minimize with respect to  $\mathbf{N}$ . The second step involves recovering  $u$  from  $\mathbf{N}$  by solving

$$\min_u \left\{ \int_{\Omega} |\nabla u| - \nabla u \cdot \mathbf{N} \, dxdy + \gamma \int_{\Omega} (f - u)^2 \, dxdy \right\}. \quad (29)$$

for suitable positive  $\gamma = 1/\alpha$ . The two-step cycle is repeated as many times as needed. Practically the convergence is fast.

For (9), we need to discuss how the first step can be completely achieved. However if we redefine  $\mathbf{N}$  as  $\mathbf{N} = \nabla u$  then,

$$\det(H(u)) = \det(\nabla \mathbf{N}) \quad (30)$$

where  $\nabla \mathbf{N}$  represents a matrix whose rows are the gradient vectors of the components of  $\mathbf{N}$  i.e. the Hessian of  $u$ . Due to the new definition of  $\mathbf{N}$ , the unit vector condition will not be necessarily satisfied everywhere in the domain. To fix this problem,  $\mathbf{N}$  is numerically enforced to be a unit vector using simple brute force at the end of the first step in every cycle.

The second order partial differential equation that needs to be solved in the first step comes from following minimization problem:

$$\min_{\mathbf{N}} R(\mathbf{N}, u) \equiv \left\{ \int_{\Omega} \left| \frac{\det(\nabla \mathbf{N})}{(|\nabla u|^2 + 1)^2} \right| dxdy \right\}. \quad (31)$$

By introducing a small vector variation  $\Psi = (\epsilon_1 \psi_1, \epsilon_2 \psi_2)^T$ , to  $\mathbf{N} = (N_1, N_2)^T$ , the first order optimality conditions for this problem can be expressed as

$$\frac{dR(\mathbf{N} + \Psi)}{d\epsilon_1} = 0 \quad \text{and} \quad \frac{dR(\mathbf{N} + \Psi)}{d\epsilon_2} = 0. \quad (32)$$

The above equations, involve differentiating the determinant of a matrix, say  $A$ , with respect a parameter  $\epsilon$ . This can be done using the following known formula:

$$\frac{d}{d\epsilon} \det A(\epsilon) = \det A(\epsilon) \text{trace} \left( (A^{-1}(\epsilon)) \frac{d}{d\epsilon} A(\epsilon) \right). \quad (33)$$

Applying (33) to (32) and after some manipulation, we obtain the Euler-Lagrange equations of (31)

$$\text{sign} \left( \frac{\det(\nabla \mathbf{N})}{(|\nabla u|^2 + 1)^2} \right) \nabla \cdot ((N_2)_y, -(N_2)_x) = 0 \quad (34)$$

$$\text{sign} \left( \frac{\det(\nabla \mathbf{N})}{(|\nabla u|^2 + 1)^2} \right) \nabla \cdot ((-N_1)_y, (N_1)_x) = 0. \quad (35)$$

The whole procedure of the TS method is summarized in Algorithm 1.

---

**Algorithm 1.** *TS method*

---

**Require:**  $u^0 = f$ ,  $\varepsilon > 0$ ,  $IN1$ ,  $IN2$ ,  $OUT$

$n = 0$ ; compute  $\mathbf{N}^0$  using  $f$

**while**  $n < OUT$  **do**

**for**  $k=0$  to  $IN1$  **do**

    With  $\mathbf{N}^n$  as initial guess, solve (34) and (35) keeping  $u^n$  lagged

$$N_1^{k+1} = N_1^k - \Delta t \left( \text{sign} \left( \frac{\det(\nabla \mathbf{N})}{(|\nabla u^n|^2 + 1)^2} \right) \nabla \cdot ((N_2)_y, -(N_2)_x) \right)$$

$$N_2^{k+1} = N_2^k - \Delta t \left( \text{sign} \left( \frac{\det(\nabla \mathbf{N})}{(|\nabla u^n|^2 + 1)^2} \right) \nabla \cdot ((-N_1)_y, (N_1)_x) \right)$$

**end for**

  Update  $\mathbf{N}$  by doing  $\mathbf{N}^{n+1} = \mathbf{N}^{IN1}$

  Normalize  $\mathbf{N} = \mathbf{N} / \|\mathbf{N}\|$

**for**  $k=0$  to  $IN2$  **do**

    With  $u^n$  as initial guess, solve the following equation keeping  $\mathbf{N}^{n+1}$  lagged

$$u^{k+1} = u^k - \Delta t \left( -\nabla \cdot \frac{\nabla u^k}{|\nabla u^k| + \varepsilon} + \nabla \cdot \mathbf{N} + \gamma(f - u^k) \right)$$

**end for**

  Update  $u^n$  by doing  $u^{n+1} = u^{IN2}$

$n = n + 1$

**end while**

where  $\varepsilon$  is a small positive value to avoid division by zero

---

Although, at present time we have no formal proof of the convergence of this method for the GC model, we will present evidence in the numerical experiments section showing that in fact this method performs very well when solving the GC model. Further, in [3] the authors provided a complete proof of convergence of the very same technique applied to a very similar problem: a variant of the Euler's elastica inpainting model and therefore a mean curvature based model. A similar convergence analysis for the GC model following the steps of [3] will be part of our future work. Last but not least, the idea of first smoothing a noisy vector field and recovering smoothed intensity values from it by interpolation has been successfully tested either for surface fairing problems in [6, 32] or image denoising and inpainting in [2, 22].

## 4.2 Augmented Lagrangian Method for the Gaussian curvature based model

Our second method is the augmented Lagrangian method (ALM) which recently has seen its popularity increased in the image processing community due to the remarkable results delivered. Some examples of its use for solving variational models can be found in [38, 9, 37, 43] and references therein.

We will proceed to show how to implement ALM for the Gaussian curvature based denoising model. To this end, we introduce some basic notation: the Euclidean space  $\mathbb{R}^{M \times N}$  of matrices  $M \times N$  is denoted as  $V$ . A gray-scale image

$u$  lives in  $V$  and its gradient  $\nabla u$  lives in  $Q = V \times V$ . To distinguish between the inner products and Euclidean norms in each space we use the following notation: we use  $(\cdot, \cdot)_V$  and  $\|\cdot\|_V$  to denote the usual inner product and Euclidean norm of  $V$  and similarly  $(\cdot, \cdot)_Q$  and  $\|\cdot\|_Q$  to denote the same in the space  $Q$ . In the latter case, they are defined as follows: for  $\mathbf{p} = (p^1, p^2) \in Q$  and  $\mathbf{q} = (q_1, q_2) \in Q$ ,  $(\mathbf{p}, \mathbf{q})_Q = (p^1, q_1)_V + (p^2, q_2)_V$  and  $\|\mathbf{p}\|_Q = \sqrt{(\mathbf{p}, \mathbf{p})_Q}$ .

To solve the GC denoising model (9) with the augmented Lagrangian method we introduce the variables  $\mathbf{p} \in Q$  and  $v \in V$  and reformulate the problem as the following constrained optimization problem

$$\begin{aligned} \min_{u \in V, \mathbf{p} \in Q} \left\{ G_{GC}(u, \mathbf{p}) = R_{GC}(u, \mathbf{p}) + \frac{\alpha}{2} \|u - f\|_V^2 \right\}, \\ \text{s.t. } \mathbf{p} = \nabla u. \end{aligned} \quad (36)$$

The augmented Lagrangian functional for the above constrained optimization problem is as follows:

$$\mathcal{L}_{GC}(v, \mathbf{q}; \boldsymbol{\mu}) = R_{GC}(v, \mathbf{q}) + \frac{\alpha}{2} \|v - f\|_V^2 + (\boldsymbol{\mu}, \mathbf{q} - \nabla v)_Q + \frac{r}{2} \|\mathbf{q} - \nabla v\|_Q^2, \quad (37)$$

where  $\boldsymbol{\mu} \in Q$  is the Lagrange multiplier and  $r$  is a positive constant. The saddle-point problem for the augmented Lagrangian method for the Gaussian curvature model is

$$\begin{aligned} \text{Find } (u, \mathbf{p}, \boldsymbol{\lambda}) \in V \times Q \times Q \\ \text{s.t. } \mathcal{L}_{GC}(u, \mathbf{p}, \boldsymbol{\mu}) \leq \mathcal{L}_{GC}(u, \mathbf{p}, \boldsymbol{\lambda}) \leq \mathcal{L}_{GC}(v, \mathbf{q}, \boldsymbol{\lambda}) \quad \forall (v, \mathbf{q}, \boldsymbol{\mu}) \in V \times Q \times Q. \end{aligned} \quad (38)$$

To solve the saddle-point problem, the iterative algorithm described in Algorithm 2 is used

---

**Algorithm 2.** *Augmented Lagrangian method for the Gaussian curvature based denoising model*

---

*Initialize*  $\boldsymbol{\lambda}^0 = \mathbf{0}$

**for**  $k=0$  to  $MAX$  **do**

*Compute*  $(u^k, \mathbf{p}^k)$  *as an approximate minimizer of the augmented Lagrangian functional with the Lagrange multiplier*  $\boldsymbol{\lambda}^k$  *i.e.,*

$$(u^k, \mathbf{p}^k) \approx \min_{(v, \mathbf{q}) \in V \times Q} \mathcal{L}_{GC}(v, \mathbf{q}; \boldsymbol{\lambda}^k), \quad (39)$$

*where*  $\mathcal{L}_{GC}(v, \mathbf{q}; \boldsymbol{\lambda}^k)$  *is defined in* (37)

*update*  $\boldsymbol{\lambda}^{k+1} = \boldsymbol{\lambda}^k + r(\mathbf{p}^k - \nabla u^k)$

**end for**

---

In Algorithm 2 we use an alternate minimization procedure to approximate the solution. This is, we solve two sub-problems, first we solve for  $u$  and second

for  $\mathbf{p}$ . This process is repeated until the following stopping criteria based on the relative error of the solution is satisfied:

$$\frac{\|u^k - u^{k-1}\|_{L^1}}{\|u^{k-1}\|_{L^1}} < \varepsilon \quad (40)$$

for predefined small  $\varepsilon > 0$ .

#### 4.2.1 Sub-problem for $u$

For a given  $\mathbf{q}$  and  $\lambda$

$$\min_{v \in V} \left\{ \frac{\alpha}{2} \|v - f\|_V^2 - (\boldsymbol{\lambda}^k, \nabla v)_Q + \frac{r}{2} \|\mathbf{q} - \nabla v\|_Q^2 \right\}. \quad (41)$$

This sub-problem can be efficiently solved using the optimality condition given by the linear PDE

$$-r\Delta v + \alpha(v - f) + \nabla \cdot \boldsymbol{\lambda}^k + r\nabla \cdot \mathbf{q} = 0. \quad (42)$$

Here we use Neumann's boundary conditions and a preconditioned conjugate gradient method to find the numerical solution. It is also possible to set periodic boundary conditions allowing to use Fourier transforms [38].

#### 4.2.2 Sub-problem for $\mathbf{p}$

For a given  $v$  and  $\lambda$

$$\min_{\mathbf{q} \in Q} \left\{ R(v, \mathbf{q}) + (\boldsymbol{\lambda}^k, \mathbf{q})_Q + \frac{r}{2} \|\mathbf{q} - \nabla v\|_Q^2 \right\}. \quad (43)$$

The optimality condition for this sub-problem, with  $\Gamma = q_1^2 + q_2^2 + 1$  is

$$- \left( \left( \frac{(q_2)_y}{\Gamma^2} \right)_x + \left( \frac{-(q_2)_x}{\Gamma^2} \right)_y \right) - \frac{4SDq_1}{\Gamma^3} + \lambda_1 + r(q_1 - v_x) = 0 \quad (44)$$

$$- \left( \left( \frac{-(q_1)_y}{\Gamma^2} \right)_x + \left( \frac{(q_1)_x}{\Gamma^2} \right)_y \right) - \frac{4SDq_2}{\Gamma^3} + \lambda_2 + r(q_2 - v_y) = 0 \quad (45)$$

where

$$\mathcal{D} = \det(\nabla(\mathbf{q})) = (q_1)_x(q_2)_y - (q_1)_y(q_2)_x, \\ \mathcal{S} = \text{sign} \left( \frac{\mathcal{D}}{(\|\nabla u\|^2 + 1)^2} \right),$$

Equations (44) and (45) can be solved for  $q_1$  and  $q_2$  with no need of any iterative procedure.

Numerous experiments over the KODAK database show enough evidence to believe that the ALM method for the GC model converges to a solution visually congruent with the minimization of the variational model introduced in (9). However a rigorous mathematical proof of convergence will be left for future work.

## 5 Experimental Results

In this section we give some evidence of the denoising properties and some results using the GC model on different images. All the results presented in this section for the GC model were obtained using the TS method with  $\varepsilon = 10^{-2}$  selected in Algorithm 1.

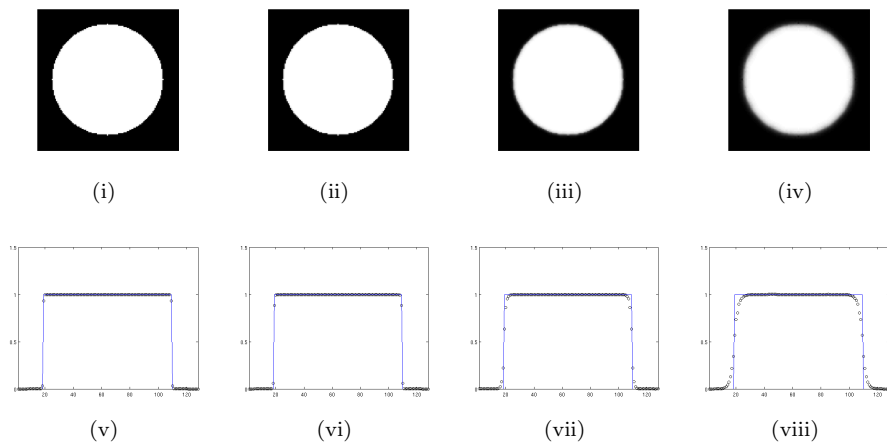


Figure 2: First row, processed images with regularizer parameter set to: (i)  $\frac{1}{2}\alpha_{max}$ , (ii)  $\alpha_{max}$ , (iii)  $2\alpha_{max}$ , (iv)  $10\alpha_{max}$ . Second row, 1D plot of one line of the image above.

**Edge preservation.** In Figure 2, we illustrate the edge preservation property of the GC model. A synthetic image containing a circular object of radius  $R = 50$  and contrast  $h = 1$  was created and the maximum allowed value for the regularization parameter  $\alpha_{max}$  computed using (23). From the first two columns in Figure 2, it can be observed that provided  $\alpha \leq \alpha_{max}$  edges remain very sharp. However for values twice and ten times  $\alpha_{max}$ , see third and fourth columns in the same Figure, edges start being rounded.

The maximum value  $\alpha_{max}$  in (23) also gives an insight about when edges will be preserved and noise will be fairly removed. Since  $\alpha_{max}$  is independent on the radius of the object, noise will be removed in same proportion no matter the size of the object. We illustrate this phenomenon in Figure 3 where two different images have been corrupted with a small quantity of Gaussian noise,  $\sigma = 5$ . We use a very low level noise in order to keep the value of  $h$  close to one, therefore the previously computed  $\alpha_{max}$  remains valid. In Figure 3(ii) we see the result of denoising a circular noisy object of radius  $R = 50$  using the GC model with the maximum allowed value for the regularization parameter. It can be appreciated that noise was fairly removed. In Figure 3(iv) we apply the same denoising procedure using the very same  $\alpha$  for the circular object of radius  $R = 250$  in the image. Again noise has been fairly removed and edges

remain sharp.

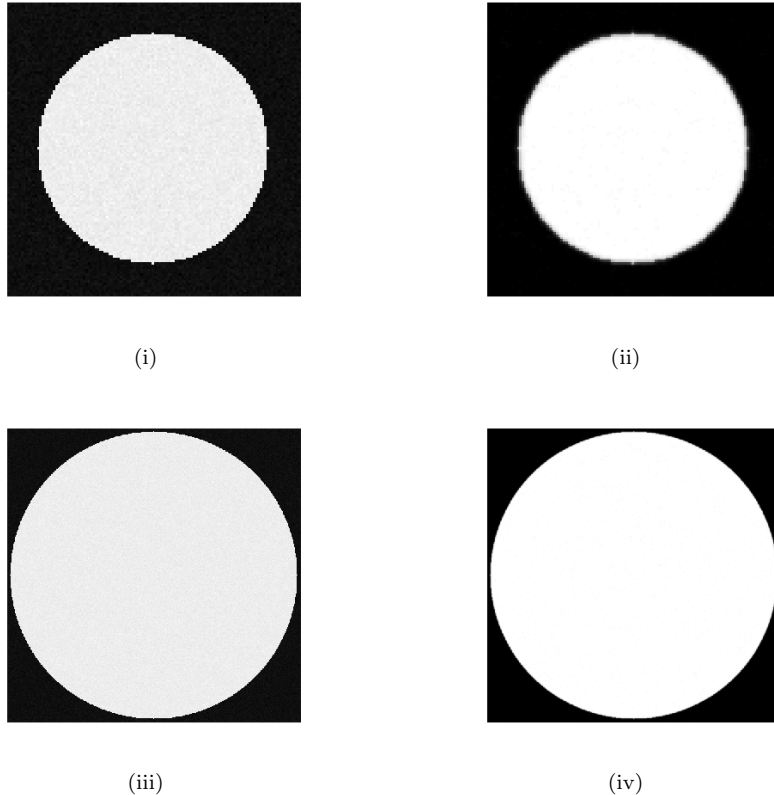


Figure 3: Two images with circles of radius  $R = 50$  and  $R = 250$  respectively. Each image has been processed with the maximum allowed value of the regularization parameter for  $R = 50$ . In both cases, noise has been removed and edges preserved.

It is important to notice that edge preservation on the GC model does not depend upon the size of the object. An opposite behavior can be found in the MC model where  $\alpha_{max} = \frac{h^4}{12R}$  and the model prefers small-sized objects and large gray scale values.

Actually, this property of the MC model is highlighted in [41] with the argument that the MC model can be used as a data-driven scale selection approach. Although certainly it is possible to use this property to ones advantage in some situations, we believe that for image denoising this may not be a nice feature. We argue that in noisy images containing objects with many different scales, one will have to select a given  $\alpha$  to guarantee noise removal but must likely this  $\alpha$  will violate the maximum allowed condition for the large objects smearing

their edges.

The GC model on the other hand does not have this problem.

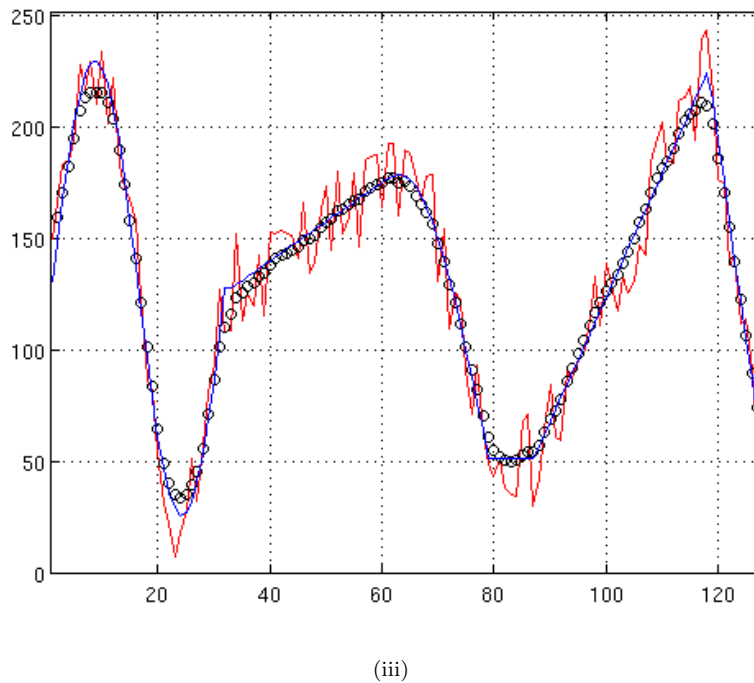
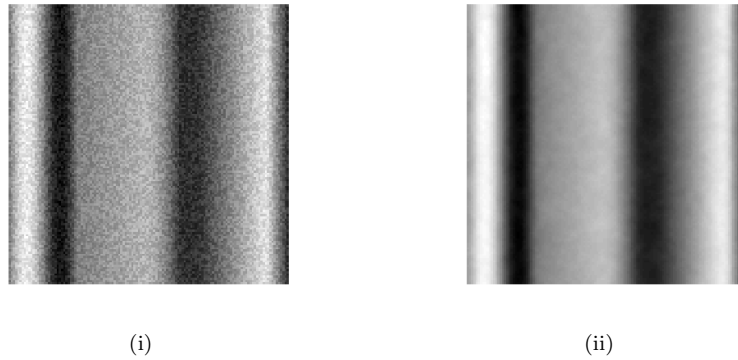


Figure 4: (i) Noisy piecewise smooth image (ii) Restored image using the GC model (iii) 1-D plot of the middle line of the images. Solid blue line is the groundtruth; solid red line is the noisy line; black circle markers are the GC result.

**Denosing of a smooth synthetic image.** In Figure 4, a noisy synthetic

piecewise smooth image has been restored with the GC model. This figure, illustrates the good performance of the GC model denoising this type of images. It can be seen that smooth regions are very well recovered by the model and noise fairly removed. Figure 4(ii) shows a visually pleasant result while the 1-D plot of any line presented in Figure 4(iii) shows how very well the solution from the GC model fits to the true image.

**Comparison of GC against popular variational models on a large database.**

To test our model, we decided to use the Kodak image database [20]. To this end, the resolution of the images was reduced by half and the luminance channel of each one computed to construct a set of gray scale images. We tested the total variation based model of Rudin, Osher and Fatemi [26] and the mean curvature based model [41] on the entire Kodak database and compared the results against those from our model. The results are presented in Figure 5 where the average increase in PSNR, computed over the entire Kodak database and using different levels of additive Gaussian noise, is presented. By increase in PSNR we mean  $PSNR(u) - PSNR(f)$  with  $u$  defined as the restored image from a given method and  $f$  as the noisy. It is evident from Figure 5 that the denoised images obtained using the Gaussian curvature model are better in terms of the PSNR than those obtained using the ROF or the mean curvature model.

To obtain the results shown in Figure 5, and in order to make a fair comparison, we used manually optimized values of  $\alpha$  for each model: for the TV model the values were very close to the known rule of thumb  $\alpha = \sigma$ ; for the GC model the best values were  $\alpha = 0.1, 0.2, 1, 10, 20$  and for the MC model were  $\sigma = 5, 10, 15, 20, 25$ .

In order to illustrate the quality of reconstruction of the GC model and to have a point of comparison against the results from the MC and TV models we are including three denoising examples in Figure 6. The noisy images in the first column of Figure 6 were created by adding Gaussian noise with  $\sigma = 15$  to the original clean images taken from the KODAK image database. Visually we can observe how the GC model preserves edges while fairly removing noise. The results from the MC model tend to have slightly smoothed edges and the background is also less clean. The results from the TV model have the well known problem of blocky regions.

**Comparison of GC and TGV models.** Finally, we compared our model against the TGV model [5]. In Figures 7(i) and (ii) we present the resulting denoised images from the TGV and GC models respectively over a test image taken from [5]. Figures 7(iii) and (iv) are 3-D surface representations of the (i) and (ii) images. Clearly no staircase can be noticed. This example highlights that the outcome from both models are comparable when restoring smooth images.

**CPU-times.** We discuss here the CPU-time of both numerical methods proposed to solve numerically our GC model: the TS and ALM methods. To get some insight, we selected two popular test images: Lena and Peppers with three different resolutions, added Gaussian noise with  $\sigma = 15$  and tested both

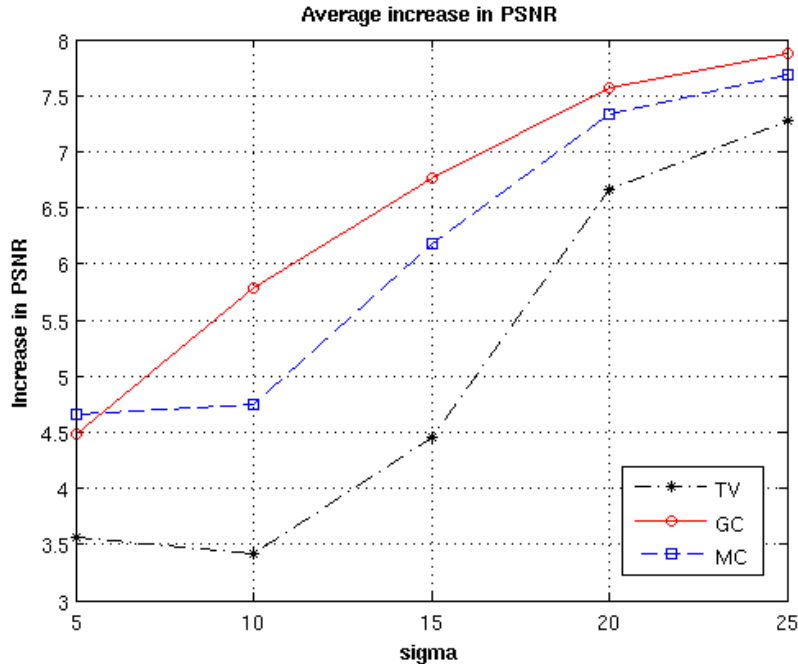


Figure 5: The average increase in PSNR computed over the entire Kodak database is shown. The GC model delivers the best average increase for all different levels of noise.

numerical methods. Overall, in the ALM method 6 cycles are needed to get convergence while the TS method needs only 5 cycles.

In Table 1 we show the average CPU-time taken to process the images for resolutions of  $128 \times 128$ ,  $256 \times 256$ , and  $512 \times 512$  pixels. As can be seen both algorithms are very fast in getting the numerical solution delivered being the augmented Lagrangian method the faster of them. However there is still room for improvement for the TS algorithm since at each inner step a simple gradient descent method is being used and 700 iterations run. As part of future work we shall explore both in a multigrid framework.

## 6 Conclusion

We have introduced in this paper a new regularizer based on the Gaussian curvature of the image surface. The use of this new regularizer for image denoising has been studied and analyzed in depth. Synthetic examples has been presented to highlight the virtues and deficiencies of this Gaussian regularizer. In addition we have presented two state of the art and fast methods for the numerical solution of the denoising model. Tests show that the GC results may have a better

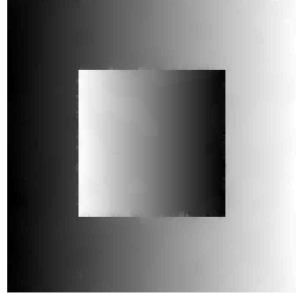


Figure 6: The noisy images in the first column have additive Gaussian noise with  $\sigma = 15$ . The results from GC model are presented in the second column. They show edge and contrast preservation as well as a fair removal of noise. The results from the MC model, in the third column, tend to have slightly smoothed edges while the background looks not as smooth as expected. The results from the TV model have the well known problem of blocky regions.

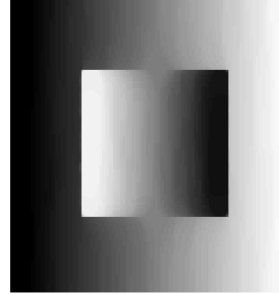
ALM			TS	
Size	CPU-time	# of Cycles	CPU-time	# of Cycles
$512 \times 512$	145.80 sec	6	791 sec	5
$256 \times 256$	17.10 sec	6	234.42 sec	5
$128 \times 128$	4.87 sec	6	51.65 sec	5

Table 1

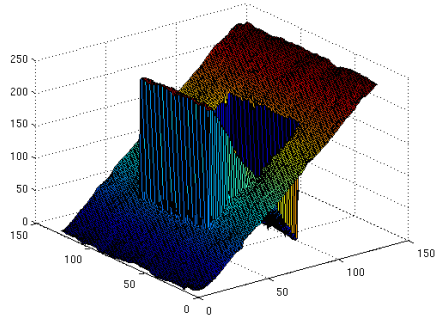
PSNR than those of the competing methods MC and TGV. Future work will explore the full potential of the new GC model or regularizer in other imaging models e.g. image registration, deblurring and segmentation to mention a few.



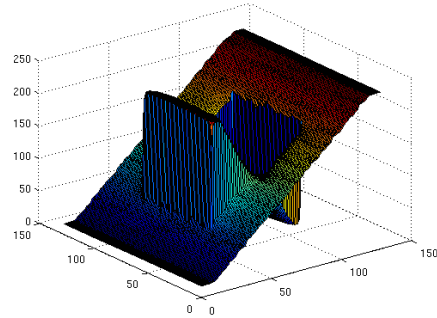
(i)



(ii)



(iii)



(iv)

Figure 7: (i) TGV result (ii) GC result (iii) 3-D surface from TGV result (iv) 3-D surface from GC result.

## Appendix A Euler-Lagrange equation

Here we derive the first order optimality condition or Euler Lagrange equation for the Gaussian curvature model already introduced in (10). In particular we concentrate on the regularization term since the first condition for the fitting term is well known. In the formal derivation we assume that the vector field  $u$  is smooth enough such that gradients are well defined and the variation  $\varphi$  has compact support over  $\Omega$  so that we can use the divergence theorem to get rid of the boundary term.

From the definition of  $R(u)$  given in (8) and since the denominator is already positive, we compute the first variation as it is customary using  $\delta R \equiv \frac{d}{d\epsilon} R(u +$

$$\begin{aligned}
& \epsilon\varphi)|_{\epsilon=0} \\
\delta R &= \left[ \frac{d}{d\epsilon} \int_{\Omega} \frac{|(u + \epsilon\varphi)_{xx}(u + \epsilon\varphi)_{yy} - (u + \epsilon\varphi)_{xy}(u + \epsilon\varphi)_{yx}|}{((u + \epsilon\varphi)_x^2 + (u + \epsilon\varphi)_y^2 + 1)^2} dx dy \right]_{\epsilon=0} \\
&= \int_{\Omega} \frac{u_{xx}u_{yy} - u_{xy}u_{yx}}{|u_{xx}u_{yy} - u_{xy}u_{yx}|} \frac{(u_{xx}\varphi_{yy} + u_{yy}\varphi_{xx} - u_{xy}\varphi_{yx} - u_{yx}\varphi_{xy})}{(u_x^2 + u_y^2 + 1)^2} dx dy \\
&\quad - \int_{\Omega} \frac{4|u_{xx}u_{yy} - u_{xy}u_{yx}|(u_x\varphi_x + u_y\varphi_y)}{(u_x^2 + u_y^2 + 1)^3} dx dy.
\end{aligned}$$

At this point we introduce new notation to simplify the writing of the equations  $\mathcal{N} = u_x^2 + u_y^2 + 1$ ,  $\mathcal{S} = \text{sign}(u_{xx}u_{yy} - u_{xy}u_{yx})$  where  $\text{sign}()$  is the sign function and  $\boldsymbol{\nu} = (\nu_1, \nu_2)$  the normal vector unit. We also make use of the divergence theorem when required

$$\begin{aligned}
\delta R &= - \int_{\Omega} \varphi \left( \frac{\mathcal{S}u_{xy}}{\mathcal{N}^2} \right)_{xy} - \int_{\partial\Omega} \varphi_y \frac{\mathcal{S}u_{xy}}{\mathcal{N}^2} \nu_1 d\Gamma + \int_{\partial\Omega} \varphi \left( \frac{\mathcal{S}u_{xy}}{\mathcal{N}^2} \right)_x \nu_2 d\Gamma \\
&\quad - \int_{\Omega} \varphi \left( \frac{\mathcal{S}u_{yx}}{\mathcal{N}^2} \right)_{yx} - \int_{\partial\Omega} \varphi_x \frac{\mathcal{S}u_{yx}}{\mathcal{N}^2} \nu_2 d\Gamma + \int_{\partial\Omega} \varphi \left( \frac{\mathcal{S}u_{yx}}{\mathcal{N}^2} \right)_y \nu_1 d\Gamma \\
&\quad + \int_{\Omega} \varphi \left( \frac{\mathcal{S}u_{xx}}{\mathcal{N}^2} \right)_{yy} + \int_{\Omega} \varphi_y \frac{\mathcal{S}u_{xx}}{\mathcal{N}^2} \nu_2 d\Gamma - \int_{\Omega} \varphi \left( \frac{\mathcal{S}u_{xx}}{\mathcal{N}^2} \right)_y \nu_2 d\Gamma \\
&\quad + \int_{\Omega} \varphi \left( \frac{\mathcal{S}u_{yy}}{\mathcal{N}^2} \right)_{xx} + \int_{\Omega} \varphi_x \frac{\mathcal{S}u_{yy}}{\mathcal{N}^2} \nu_1 d\Gamma - \int_{\Omega} \varphi \left( \frac{\mathcal{S}u_{yy}}{\mathcal{N}^2} \right)_x \nu_1 d\Gamma \\
&\quad + \int_{\Omega} \varphi \left( \frac{4|u_{xx}u_{yy} - u_{xy}u_{yx}|u_x}{\mathcal{N}^3} \right)_x - \int_{\partial\Omega} \left( \frac{4|u_{xy}^2 - u_{xx}u_{yy}|u_x}{\mathcal{N}^3} \right) \nu_1 d\Gamma \\
&\quad + \int_{\Omega} \varphi \left( \frac{4|u_{xx}u_{yy} - u_{xy}u_{yx}|u_y}{\mathcal{N}^3} \right)_y - \int_{\partial\Omega} \left( \frac{4|u_{xx}u_{yy} - u_{xy}u_{yx}|u_y}{\mathcal{N}^3} \right) \nu_2 d\Gamma.
\end{aligned}$$

In order to drop the boundary terms we ask for

$$\begin{aligned}
& (-u_{xy}, u_{xx}) \cdot \boldsymbol{\nu} = 0, (u_{yy}, -u_{yx}) \cdot \boldsymbol{\nu} = 0, \\
& \left( \left( \frac{\mathcal{S}u_{yx}}{\mathcal{N}^2} \right)_y, - \left( \frac{\mathcal{S}u_{xx}}{\mathcal{N}^2} \right)_y \right) \cdot \boldsymbol{\nu} = 0, \left( - \left( \frac{\mathcal{S}u_{yy}}{\mathcal{N}^2} \right)_x, \left( \frac{\mathcal{S}u_{xy}}{\mathcal{N}^2} \right)_x \right) \cdot \boldsymbol{\nu} = 0
\end{aligned}$$

Finally, by defining

$$\mathbf{B}_1 = \left( \left( \frac{\mathcal{S}u_{yy}}{\mathcal{N}^2} \right)_x, \left( - \frac{\mathcal{S}u_{xy}}{\mathcal{N}^2} \right)_x \right) \quad (46)$$

$$\mathbf{B}_2 = \left( - \left( \frac{\mathcal{S}u_{yx}}{\mathcal{N}^2} \right)_y, \left( \frac{\mathcal{S}u_{xx}}{\mathcal{N}^2} \right)_y \right) \quad (47)$$

it is possible to write the Euler Lagrange equation for the GC model as

$$\alpha \nabla \cdot \left( \frac{4|u_{xx}u_{yy} - u_{xy}u_{yx}|}{\mathcal{N}^3} \nabla u \right) + \nabla \cdot \mathbf{B}_1 + \nabla \cdot \mathbf{B}_2 + u - f = 0 \quad (48)$$

with the above boundary conditions.

## Appendix B GC as a function of $g$

Here we will give a proof for (11). First we compute the derivatives in terms of  $g$

$$\begin{aligned}
 u_x &= g' \frac{x}{r}, \\
 u_y &= g' \frac{y}{r}, \\
 u_{xx} &= g'' \frac{x^2}{r^2} + g' \frac{y^2}{r^3}, \\
 u_{yy} &= g'' \frac{y^2}{r^2} + g' \frac{x^2}{r^3}, \\
 u_{xy} &= u_{yx} = g'' \frac{xy}{r^2} - g' \frac{xy}{r^3}, \\
 1 + u_x^2 + u_y^2 &= 1 + (g')^2.
 \end{aligned}$$

Using the above in (7) we get

$$\begin{aligned}
 \kappa_G &= \frac{u_{xx}u_{yy} - u_{xy}u_{yx}}{(1 + u_x^2 + u_y^2)^2}, \\
 &= \frac{(g'' \frac{x^2}{r^2} + g' \frac{y^2}{r^3})(g'' \frac{y^2}{r^2} + g' \frac{x^2}{r^3}) - (g'' \frac{xy}{r^2} - g' \frac{xy}{r^3})^2}{(1 + (g')^2)^2}, \\
 &= \frac{(g' g'' \frac{x^4}{r^5} + 2g' g'' \frac{x^2 y^2}{r^5} + g' g'' \frac{y^4}{r^5})}{(1 + (g')^2)^2}, \\
 &= \frac{g' g''}{r^5 (1 + (g')^2)^2} (x^4 + 2x^2 y^2 + y^4), \\
 &= \frac{g' g''}{r^5 (1 + (g')^2)^2} (x^2 + y^2)^2, \\
 &= \frac{g' g''}{r^5 (1 + (g')^2)^2} (r^2)^2, \\
 &= \frac{g' g''}{r (1 + (g')^2)^2}.
 \end{aligned}$$

This completes the proof.

## References

- [1] G. Aubert and P. Kornprobst. Mathematical Problems In Image Processing - Partial Differential Equations And The Calculus Of Variations. *Springer Applied Mathematical Sciences*, Vol. 147, 2002.
- [2] C. Ballester, M. Bertalmio, V. Caselles, G. Sapiro, and J. Verdera, Filling-in by joint interpolation of vector fields and gray levels. *IEEE Trans. Image Process.*, 10(8) (2001), pp. 1200–1211

- [3] C. Ballester, V. Caselles, and J. Verdera, Disocclusion by joint interpolation of vector fields and gray levels. *Multiscale Modeling & Simulation*, 2(1) (2003), 80-123.
- [4] M. Bertalmío, S. Levine, Denoising an Image by Denoising its Curvature Image *SIAM J. Imaging Sci.*, 7(1), (2013), pp. 187–211.
- [5] Kristian Bredies, Karl Kunisch and Thomas Pock. Total generalized variation. *SIAM Journal on Imaging Sciences*, 3(3):492-526, 2010.
- [6] Carlos Brito-Loeza and Ke Chen. Fast iterative algorithms for solving the minimization of curvature-related functionals in surface fairing. *International Journal of Computer Mathematics*, Vol. 90, Iss. 1, 2013.
- [7] Carlos Brito-Loeza and Ke Chen. Multigrid Algorithm for High Order Denoising. *SIAM Journal on Imaging Sciences*, Volume 3 (3), pp.363-389, 2010.
- [8] Tony F. Chan, Sung Ha Kang and Jianhong Shen. Euler’s elastica and curvature based inpaintings. *SIAM J. Appl. Math.*, 63(2):564–592, 2002.
- [9] S. H. Chan, Khoshabeh, R., Gibson, K. B., Gill, P. E., and Nguyen, T. Q. An augmented Lagrangian method for total variation video restoration. *IEEE Transactions on Image Processing*, vol. 20, no. 11, pp. 3097-3111, 2011.
- [10] Chunchob Noppadol, Ke Chen and Carlos Brito-Loeza. A fourth order variational image registration model and its fast multigrid algorithm. *SIAM J. Multiscale Modeling and Simulation*, Vol 9 (1), pp.89-128, 2011.
- [11] Ke Chen and Joseph Savage. An accelerated algebraic multigrid algorithm for total variation denoising. *BIT Numerical Mathematics*, 47:277–296, 2007.
- [12] Yunmei Chen, Stacey Levine and Murali Rao. Variable exponent, linear growth functionals in image restoration. *SIAM J. Appl. Math.*, 66(4):1383–1406, 2006.
- [13] R.A. DeVore and B.J. Lucier. Fast wavelet techniques for near-optimal processing. *IEEE Military Communications Conference*, 48.3.1-48.3.7, 1992.
- [14] D.L. Donoho and I.M. Jhonstone Adapting to unknown smoothness via wavelet shrinkage. *Journal of the American Statistical Association*, 90, 1200-1224, 1995.
- [15] M. Elsey and S. Esedoglu. Analogue of the total variation denoising model in the context of geometry processing. *SIAM J. Multiscale Modeling and Simulation*. 7:4 (2009), pp. 1549-1573.
- [16] F L Yang, Ke Chen and Bo Yu. Homotopy method for a mean curvature-based denoising model. *Journal of Applied Numerical Mathematics*, Vol 62 (3), pp.185-200, 2012.
- [17] R. Goldman. Curvature formulas for implicit curves and surfaces. *Computer Aided Geometric Design*, 22 (2005) 632–658.
- [18] T. Goldstein and S. Osher. The split Bregman method for L1-regularized problems. *SIAM J. Imaging Sciences*, 2, 323-343, 2009.

- [19] Rafael Gonzalez and Richard Woods. *Digital Image Processing*. Prentice Hall; 3rd. edition, 2007.
- [20] Kodak database, “<http://r0k.us/graphics/kodak/>”.
- [21] M. Lysacker, Arvid Lundervold and Xue-Cheng Tai. Noise removal using fourth-order partial differential equation with applications to medical magnetic resonance images in space and time. *IEEE Trans. Image Proc.*, 12(12):1579–1590, 2003.
- [22] M. Lysacker, S. Osher and Xue-Cheng Tai. Noise removal using smoothed normals and surface fitting. *IEEE Trans. Image Proc.*, 13(10):1345–1357, 2004.
- [23] A. Marquina and S. Osher. Explicit algorithms for a new time dependent model based on level set motion for nonlinear deblurring and noise removal. *SIAM J. Sci. Comput.*, 22(2):387–405, 2000.
- [24] Simon Masnou and Jean-Michel Morel. Level Lines Based Disocclusion. *Proceedings of 5th IEEE International Conference on Image Processing, Chicago*, 12(7):259–263, 1998.
- [25] P. Perona and J. Malik. Scale-space and edge detection using anisotropic diffusion *IEEE Transactions on Pattern Analysis and Machine Intelligence*, 12(7):629–639, 1990.
- [26] L. I. Rudin, S. Osher, and E. Fatemi. Nonlinear total variation based noise removal algorithms. *Physica D*, 60:259–268, 1992.
- [27] Joseph Savage and Ke Chen. On multigrids for solving a class of improved total variation based staircasing reduction models. In: *”Image Processing Based On Partial Differential Equations”*, eds. X.-C. Tai, K.-A. Lie, T.F. Chan and S. Osher, pp.69-94, Springer-Verlag, 2006.
- [28] O. Scherzer, M. Grasmair, H. Grossauer, M. Haltmeier and F. Lenzen. *Variational methods in imaging*. Applied Mathematical Sciences Volume 167, Springer, 2009.
- [29] Li Sun and Ke Chen. A New Iterative Algorithm for Mean Curvature-based Variational Image Denoising. *BIT Numerical Mathematics*, 54(2), (2014), pp 523-553.
- [30] David Strong and Tony Chan. Edge-preserving and scale-dependent properties of total variation regularization. *Inverse Problems*, 19(6) S165-S187, 2003.
- [31] Q Chang, XC Tai, L Xing. A compound algorithm of denoising using second-order and fourth-order partial differential equations. *Numer. Math. Theory Methods Appl*, 2, 353-376, 2009.
- [32] T. Tasdizen, R. Whitaker, P. Burchard, and S. Osher. Geometric Surface Processing via Normal Maps *ACM Trans. Graph.*, 22(4) (2003), pp. 1012–1033
- [33] L. A. Vese and S. Osher, *Numerical methods for p-harmonic flows and applications to image processing*, *SIAM J. Numer. Anal.*, 40(6):2085-2104, 2002.

- [34] Wang Chaohui, Nikos Komodakis, and Nikos Paragios. Markov Random Field modeling, inference and learning in computer vision and image understanding: A survey. *Computer Vision and Image Understanding*, 117(11), 1610-1627, 2013.
- [35] J. Weickert, Ter Haar Romeny, B.M., and M. Viergever. Efficient and reliable schemes for nonlinear diffusion filtering. *IEEE Trans. Image Processing*, 7, 398-410, 1998.
- [36] J.B Weaver, X. Yansun, D.M. Healy Jr., and L.D. Cromwell. Filtering noise from images with wavelet transforms. *Magnetic Resonance in Medicine*, 24, 288-295, 1991.
- [37] C. Wu, and X-C. Tai. Augmented Lagrangian Method, Dual Methods, and Split Bregman Iteration for ROF, Vectorial TV, and High Order Models. *SIAM Journal on Imaging Sciences.*, 3:3, 300-339, 2010.
- [38] C. Wu, J. Zhang and X-C. Tai. Augmented Lagrangian method for total variation restoration with non-quadratic fidelity. *Inverse Problems and Imaging*, 5(1):237–261, 2011.
- [39] Yu-Li You and M. Kaveh. Fourth-order partial differential equations for noise removal. *IEEE Trans. Image Proc.*, 9(10):1723–1730, 2000.
- [40] J P Zhang, Ke Chen and Bo Yu. An Iterative Lagrange Multiplier Method for Constrained Total Variation-Based Image Denoising. *SIAM J. Imaging Sci.*, 5(3), 983-1003, 2012.
- [41] Wei Zhu and Tony Chan. Image denoising using mean curvature of image surface. *SIAM J. Imaging Sci.*, 5, pp. 1-32, 2012.
- [42] Zhu, W.; Chan, T. F.; Esedoglu. Segmentation with depth: A level set approach. *SIAM Journal on Scientific Computing.*, 28(5), 1957–1973, 2006. SIAM Journal on Scientific Computing archive
- [43] Wei Zhu, Xue Cheng Tai, and Tony Chan. Augmented Lagrangian method for a mean curvature based image denoising model. *Inverse Problems and Imaging*, 7(4), (2013), pp 1409-1432.